

Morphology, structure and electrical properties of iron nanochains

T P Huelser¹, H Wiggers², P Ifeacho², O Dmitrieva¹, G Dumpich¹
and A Lorke¹

¹ Institute of Physics, University Duisburg Essen, 47057 Duisburg, Germany

² Institute of Combustion and Gasdynamic, University Duisburg-Essen, 47057 Duisburg, Germany

E-mail: huelser@ivg.uni-duisburg.de, wiggers@uni-duisburg.de and axel.lorke@uni-due.de

Received 28 February 2006

Published 5 June 2006

Online at stacks.iop.org/Nano/17/3111

Abstract

Iron nanoparticles with a diameter of 35 nm are synthesized by the thermal decomposition of iron pentacarbonyl in a hot wall reactor. The particles are ferromagnetic and single magnetic domain. The magnetic forces between the particles cause the formation of iron nanowires of up to 300 μm in length. Morphological characterization using high resolution transmission electron microscopy indicates an oxidic shell with a thickness of 3–4 nm. The electrical properties of single chains are investigated under air using impedance spectroscopy (IS). It is found that the conductivity of the iron is in the same range as that of the bulk material. Temperature dependent measurements on iron nanochain powders performed under H_2 -atmosphere reveal strong sintering effects and a transition into iron.

1. Introduction

Driven by improved synthesis routes and characterization methods, high quality, structured ferromagnetic particles have become available in recent years [1–3]. Iron based nanomaterials such as iron oxides have been synthesized and intensively characterized with special emphasis on structure, magnetism and electrical properties [4, 5]. Because of quantum and other size effects, the properties of nano-sized oxidic materials differ from those of the bulk [6, 7]. Iron is of particular interest because its high magnetic moment combined with its metallic conductivity, opens up numerous applications [8, 9]. For realizing high magnetizations in these systems, the aim must be to increase the amount of the ferromagnetic iron phase in these systems, but due to its base metal characteristic, pure iron and especially nano-sized iron is very reactive and must be stabilized. A very simple but successful way is a slight controlled oxidation of the surface. The synthesis and formation of single-magnetic-domain iron particles, which are agglomerated in chains, was described previously by Knipping *et al* [10]. Because of their unique properties these iron chains are candidates for various applications in the future. This study focuses on the structure, morphology and the electrical properties of such self-assembled iron nanochains.

2. Experimental details

Metallic iron nanoparticles are synthesized by thermal dissociation of iron pentacarbonyl (IPC) [10]. The experimental set-up consists of a hot wall flow reactor and a filter device to collect the as-prepared particles. A mixture of IPC and N_2 as diluent is injected by a nozzle at the top of the furnace. The formation, growth and *in situ* characterization is described in detail by Knipping *et al* [10]. For particles with diameters larger than 15 nm, an agglomeration into nanochains occurs, which is driven by magnetic interactions. The iron particles investigated here are synthesized at 673 K at a pressure of 500 mbar. A pneumatic particle sampling system is used to deposit material directly out of the reactor onto transmission electron microscopy (TEM) grids and silicon wafers.

The morphological and structural properties of iron nanoparticles are investigated using high resolution TEM (HRTEM), scanning electron microscopy (SEM), and electron energy loss spectroscopy (EELS) analysis. X-ray diffraction (XRD) measurements are used to study the crystal structure and phase composition of the product. The electrical properties are investigated using impedance spectroscopy (IS) methods.

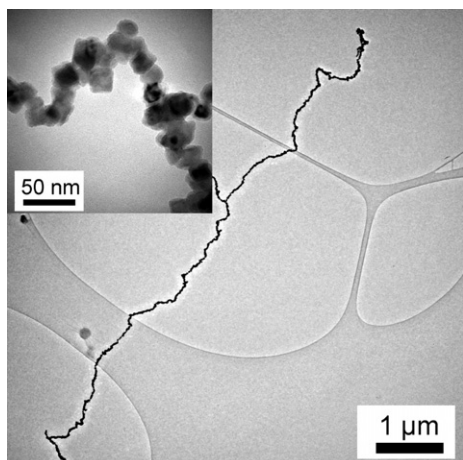


Figure 1. Thermophoretically sampled iron chain bridging the holes in a holey carbon TEM grid. The inset shows a magnification of the chain consisting of single shaped faceted particles.

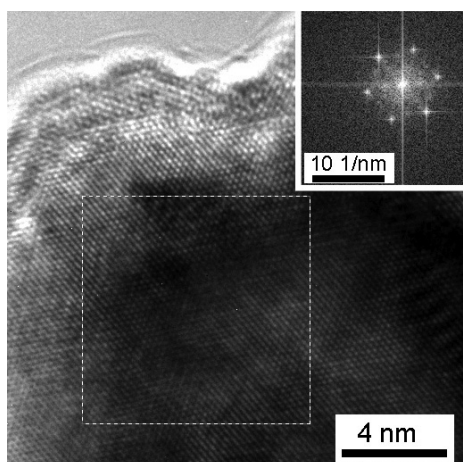


Figure 2. HRTEM image of a single iron particle in a hole of a holey carbon TEM grid. The inset shows the Fourier transformation of the crystalline area in the dashed box.

3. Results and discussion

3.1. Morphology and structure

Morphology, structure and phase composition are analysed using the imaging technology of HRTEM and SEM. The images reveal an agglomeration of single particles in chains (see figures 1 and 8(a)). Model calculations show that the chain formation can be explained by a magnetic interaction between the ferromagnetic particles in the reaction zone and additionally during the flight time before sampling [11]. Figure 1 shows a TEM image of an iron chain on a holey carbon TEM grid. The long chains can bridge the voids in the carbon layer without rupture and remain remarkably stable, thereby providing a good opportunity for detailed HRTEM investigations. Single chains have been found with lengths of up to 300 μm . Shorter and more dendritic chains were found by Huber *et al* [12]. The inset in figure 1 shows a higher magnification image which reveals that the chains consist of single shaped particles. The primary particles forming the

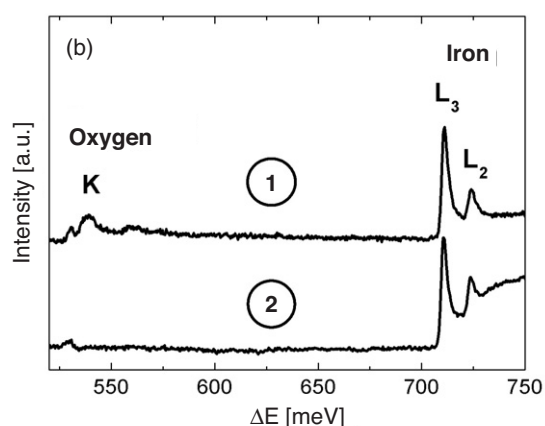
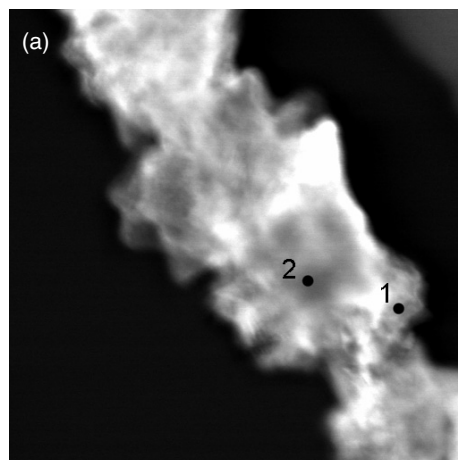


Figure 3. (a) STEM image of a particle within an iron chain. The numbered points mark the position of the EEL spectra. (b) EEL spectra of the two positions shown in (a). The measured signals can be assigned to the oxygen K_1 and the iron $L_{2/3}$ edges.

chains have a diameter of about 35 nm, and they exhibit a rectangular facet structure.

The attractive magnetic forces between the ferromagnetic particles as well as van der Waals interactions are responsible for the intergranular stability of the chains. Figure 2 shows a HRTEM image of a single iron particle. The border of the particle exhibits a brighter contrast than the centre. This can be attributed to the presence of an iron oxide shell encapsulating the iron core. The Fourier transformation of the crystalline area marked by the dashed box is shown in the inset. A lattice spacing of $d = 0.20$ nm was calculated using the distance between the spots in the Fourier representation. This value is in good agreement with the 110 lattice spacing of iron, $d_{110} = 0.2026$ nm.

EELS analysis was performed for a more element-specific investigation. Figure 3(a) shows a scanning TEM (STEM) image of a selected area of an iron chain obtained using a high-angle annular dark-field detector. The numbered dots mark the positions of the EELS point measurements taken at position 1 in the shell of the particle and at position 2 in the centre area of the particle. Figure 3(b) shows the background-subtracted energy loss spectra at these two positions. The label K indicates the energetic position of the oxygen K 1s electron binding energy [13]. L_2 and L_3 define the $2p_{1/2}$ and

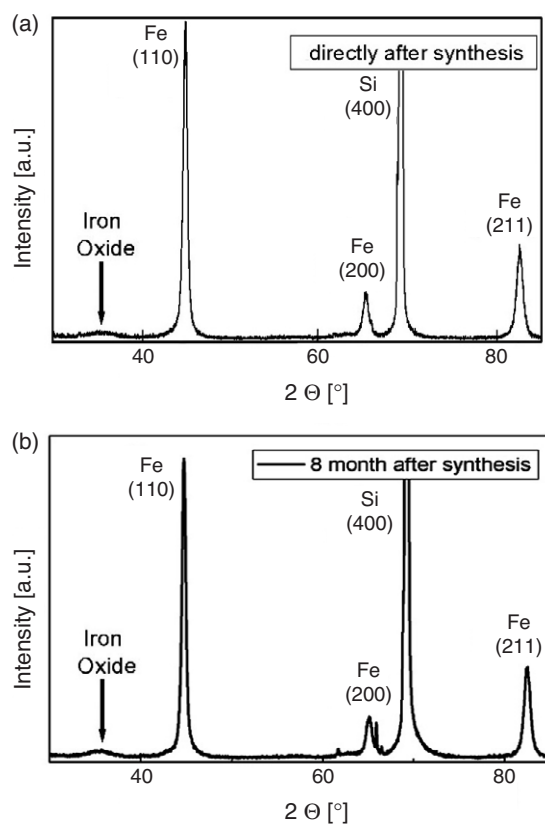


Figure 4. (a) XRD measurement of the iron chains directly after the synthesis. (b) XRD measurement of the same powder after storage under ambient atmosphere for 8 months.

$2p_{3/2}$ binding energies of iron, respectively [14]. The spectrum received from scan position 2 reveals a clear iron signal (L_3 and L_2 edges) in the energy range between 710 and 725 meV. The slight increase of intensity that can be seen at energies above the L_3 edge is caused by electron scattering processes. The K edge of oxygen is very weak in spectrum 2. This oxygen contribution originates from the oxidic shell, which encapsulates the chains. The oxygen K edge in spectrum 1 is clearly visible and its shape is typical for iron oxides [15]. It should also be noted that the intensity for energies higher than that of the L_3 edge remains constant, and therefore less electron scattering processes in the shell area are assumed. Therefore, the EEL-Spectrum at position 1 confirms the existence of iron oxide.

The temporal stability as well as the structure of the iron chain powder (see figure 8 (left)) was analysed using several XRD measurements. Figure 4(a) shows the diffraction image of the powder taken directly after the synthesis. The measurement was performed on a silicon wafer with a (400) $\text{Cu K}\alpha_1$ reflex at 69.2° . Additionally, a broad maximum with low intensity in the range of $2\Theta = 35^\circ$ was detected, which can be assigned to the (313) reflex of maghemite (Fe_2O_3) and the (311) reflex of magnetite (Fe_3O_4) [16, 17]. This signal can be attributed to the oxidic shell of the particles.

To assert the long term stability, iron chains which had been stored under ambient conditions for eight months were also investigated. Figure 4(b) shows the diffraction pattern of the stored material. Both spectra reveal the presence of

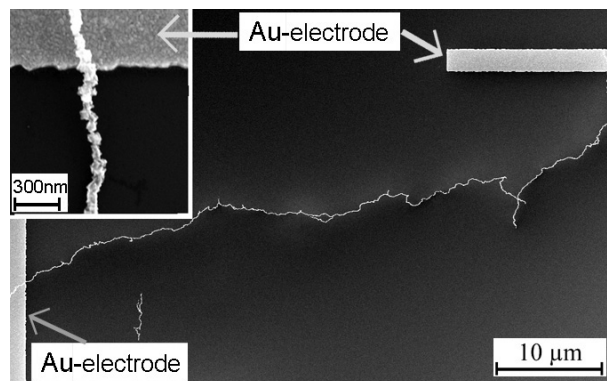


Figure 5. SEM image of an iron wire between Au electrodes on a silicon substrate. The inset shows a magnified view of the wire on the gold electrode.

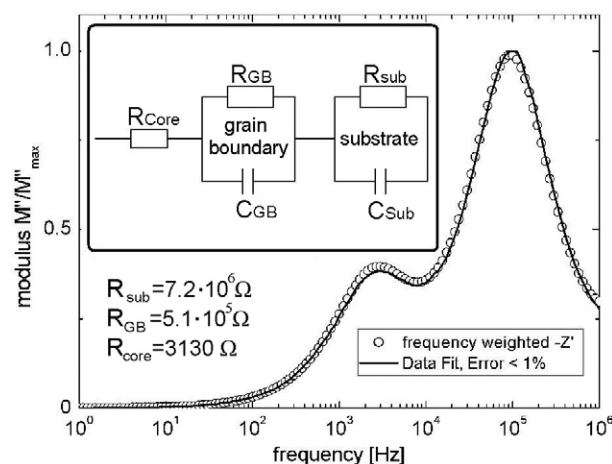


Figure 6. Normalized modulus function of an impedance spectroscopy measurement on iron nanowires at room temperature in air. The inset shows the equivalent circuit used for the data fit.

crystalline bcc iron as well as a small amount of iron oxide phases with a weak crystallinity. These measurements clearly show, that iron chains remain stable for long periods under ambient conditions.

3.2. Electrical characterization

For the impedance measurements, a Solartron SI 1255 frequency response analyser (FRA) in combination with a dielectric interface SI 1296 was used in the frequency range between 1 Hz and 1 MHz. For the investigation of the (macroscopic) material properties, samples were pressed into small discs with 5 mm diameter and 0.23 mm height. For single wire characterization, interdigital structures with a width of $2\ \mu\text{m}$ and a distance of $20\ \mu\text{m}$ are used on a slightly conducting p-type Si substrate (figure 5). Impedance spectroscopy on single chains was performed under air at room temperature with an applied AC voltage of 100 mV.

Figure 6 shows the result of an IS measurement of a single $60\ \mu\text{m}$ long nanochain, consisting of 35 nm diameter particles. For such a measurement, three different contributions to the overall conduction are taken into account in the simulation

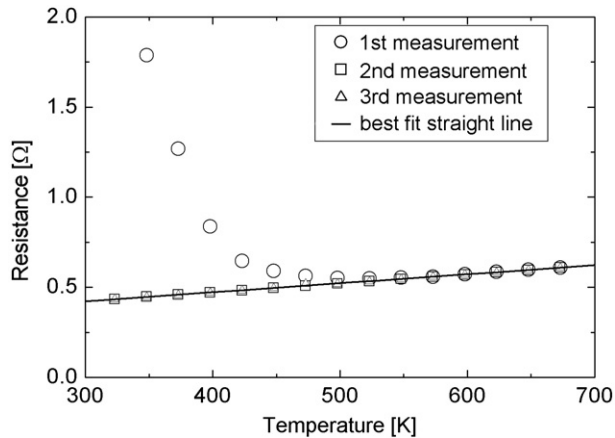


Figure 7. Temperature dependent resistance of the pressed iron wires under H_2 atmosphere. Measurements were taken at intervals of 25 K.

procedure (see inset to figure 6). The first element, R_{core} , represents the ohmic resistance of the particles, which is contributed by the iron core, the second is a parallel ($R_{\text{GB}}C_{\text{GB}}$) element for the intergranular contact between adjacent particles across the less conducting iron oxide shell. The third element ($R_{\text{sub}}C_{\text{sub}}$) accounts for the semi-conducting substrate.

In the diagram the frequency-weighted modulus M''/M''_{max} (dots) is plotted as a function of the frequency f . The data are fitted using a non linear least square fitting algorithm, the fit-results (line) are in very good agreement with the measured signal. ($R = 0.99$; note that not the shape of the curve, but each point in the complex plane is accurately reproduced by the fit). From this fit, $R_{\text{core}} = 3130 \Omega$ and $R_{\text{GB}} = 5.10 \times 10^5 \Omega$ are determined. The contribution $R_{\text{sub}} = 7.15 \times 10^6 \Omega$ is about 10 times larger than the overall impedance of the nanowire, and so only slightly affects the results of the iron chain received from lower frequency ranges. Assuming 35 nm particles with 3 nm shells, the specific resistance of the iron in the particle chain calculated from R_{core} is $5.4 \times 10^{-8} \Omega \text{ m}$. This is in good agreement with the specific resistance of bulk iron ($8.9 \times 10^{-8} \Omega \text{ m}$) [18] in the same temperature range, and further confirms our model of iron oxide covered iron particles.

As we will show in the following, the oxide shell can easily be converted into elemental iron by an annealing step under hydrogen atmosphere. Figure 7 shows the resistance of the pressed discs under hydrogen exposure in the temperature range between 323 and 673 K in steps of 25 K for three measurement cycles. The first measurement (\circ) shows an exponential decrease of the resistance with increasing temperature up to 523 K, followed by a linear increase up to 673 K. Then, the sample has been slowly cooled down to 323 K without measuring. The second measurement (\square) shows the resistance of the sample during the second heat-up cycle from 323 to 673 K, the same procedure has been applied for the third measurement cycle (\triangle). Both, the second and the third measurements reveal an increasing resistance with increasing temperature. The decrease in resistance in the first cycle indicates the reduction of iron oxide on the surface into iron. The specific resistance of ferrites is expected to be 20 times larger than that of metallic iron. A reduction of the iron oxide into iron at 523 K can be assumed because of the linear increase at higher temperatures. A linear increase in resistance with

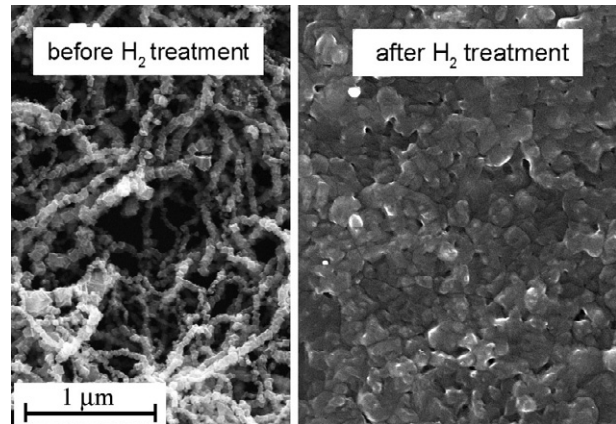


Figure 8. SEM images of the iron chains before (left) and after (right) thermal treatment under H_2 -atmosphere.

increasing temperature is caused by phonon scattering and can be observed in pure metals. The second and third measurement verify this observation and show linear behaviour in the whole temperature range as is expected for a metal. Furthermore, a simultaneous shrinkage of the sample from 5 mm in diameter into a disc of 3 mm in diameter is observable, in agreement with results reported by Sakka *et al* [19].

Figure 8 shows the surface of the pressed discs before (left) and after (right) thermal treatment under H_2 atmosphere. The chains were sintered, and thereby reduced into iron with a thin film like surface. From the dimensions and the weight of the shrunk disc, its density was calculated and found to be 13% smaller than the value of bulk iron. Therefore, holes inside the sample, which lead to larger volumes, must be assumed.

4. Conclusions

In this study, detailed investigations of the morphology and electric properties of self-assembled particulate iron nanochains are presented. Both the morphological and structural results reveal the existence of an iron core covered with an oxidic layer of about 3.5 nm. From the electrical measurements on single chains we derive an electrical conductivity of the iron cores, which agrees well with the conductivity of bulk iron. Temperature dependent IS measurements, under hydrogen atmosphere, of iron chain powder are presented. These measurements substantiate a reduction into stable iron with the electrical behaviour of a metal.

Acknowledgments

Valuable discussions with Dr Hermann Nienhaus, Institute of Physics, University Duisburg-Essen, are gratefully acknowledged. This work is supported by the Deutsche Forschungsgemeinschaft within the Sonderforschungsbereich 445.

References

- [1] Shao H, Lee H, Huang Y, Ko I and Kim C 2005 *IEEE Trans. Magn.* **41** 3388
- [2] Pei W, Kakibe S, Ohta I and Takahashi M 2005 *IEEE Trans. Magn.* **41** 3391

- [3] Miguel O B, Morales M P, Serna C J and Veintemillas-Verdaguer S 2002 *IEEE Trans. Magn.* **38** 2616
- [4] Zhang W-X 2003 *J. Nanopart. Res.* **5** 323
- [5] Suslick K S, Fang M and Hyeon T 1996 *J. Am. Chem. Soc.* **118** 11960
- [6] Chatterjee J, Haik Y and Chen C J 2003 *J. Magn. Magn. Mater.* **257** 113
- [7] Bødker F, Mørup S and Linderøth S 1994 *Phys. Rev. Lett.* **72** 282
- [8] Jordan A, Scholtz R, Wust P, Föhling H and Felix R 1999 *J. Magn. Magn. Mater.* **201** 413
- [9] Weller D, Moser A, Folks L, Best M E, Lee W, Toney M F, Schwickert M, Thiele J U and Doerner M F 2000 *IEEE Trans. Magn.* **36** 10
- [10] Knipping J, Wiggers H, Kock B F, Hülser T, Rellinghaus B and Roth P 2004 *Nanotechnology* **15** 1665
- [11] Buschmann S, Hucht A and Entel P 2006 *Phys. Rev. Lett.* submitted
- [12] Huber D L, Venturini E L, Martin J E, Provenico P P and Patel R J 2004 *J. Magn. Magn. Mater.* **278** 311
- [13] Cardona M and Ley L 1978 *Photoemission in Solids* (Berlin: Springer)
- [14] Fuggle J C and Martensson N 1980 *J. Electron. Spectrosc. Relat. Phenom.* **21** 275
- [15] Krivanek O L and Ahn C C 1983 *Gatan EELS Atlas*
- [16] Kuhn L T, Bojesen A, Timmermann L, Nielsen M M and Mørup S 2002 *J. Phys.: Condens. Matter* **14** 13551
- [17] Shmakov A N, Kryukova G N, Tsybulya S V, Chuvilin A L and Solovyeva L P 1995 *J. Appl. Crystallogr.* **28** 141
- [18] Ashcroft N W and Mermin N D 1976 *Solid State Physics* (Philadelphia, PA: Saunders)
- [19] Sakka Y, Uchikoshi T and Ozawa E 1993 *J. Mater. Sci.* **28** 203